High Power Laser Science and Engineering, (2023), Vol. 11, e46, 8 pages.
doi:10.1017/hpl.2023.31

HIGH POWER LASER SCIENCE AND ENGINEERING

RESEARCH ARTICLE

Pulse repetition-rate effect on the intensity inside a femtosecond laser filament in air

Fukang Yin[1,2], Juan Long[1,2], Yaoxiang Liu[1], Yingxia Wei[1], Bin Zhu[3], Kainan Zhou[3], Tie-Jun Wang[1,2], Yuxin Leng[1,2], and Ruxin Li[1,2]

[1] *State Key Laboratory of High Field Laser Physics, Shanghai Institute of Optics and Fine Mechanics and CAS Center for Excellence in Ultra-intense Laser Science, Chinese Academy of Sciences, Shanghai, China*

[2] *Center of Materials Science and Optoelectronics Engineering, University of Chinese Academy of Sciences, Beijing, China*

[3] *Laser Fusion Research Center and Science & Technology on Plasma Physics Laboratory, China Academy of Engineering Physics, Mianyang, China*

(Received 5 January 2023; revised 21 February 2023; accepted 24 March 2023)

Abstract

As intense, ultrashort, kHz-repetition-rate laser systems become commercially available, pulse cumulative effects are critical for laser filament-based applications. In this work, the pulse repetition-rate effect on femtosecond laser filamentation in air was investigated both numerically and experimentally. The pulse repetition-rate effect has negligible influence at the leading edge of the filament. Clear intensity enhancement from a high-repetition pulse is observed at the peak and tailing edge of the laser filament. As the repetition rate of the laser pulses increases from 100 to 1000 Hz, the length of the filament extends and the intensity inside the filament increases. A physical picture based on the pulse repetition-rate dependent 'low-density hole' effect on filamentation is proposed to explain the obtained results well.

Keywords: clamping intensity; cumulative effects; femtosecond laser filamentation

1. Introduction

A nonlinear propagation known as filamentation is produced when intense femtosecond laser pulses propagate in air. The dynamic equilibrium between the Kerr self-focusing and plasma-defocusing effects leads to filamentation[1–3]. Due to its potential applications in supercontinuum emission[4–6], extreme ultraviolet (EUV) emission[7,8], air lasing[9,10], THz radiation[11,12], remote sensing[13], guiding of corona discharges[14], machining[15] and weather control[16], filamentation of femtosecond laser pulses in optically transparent media has attracted a great deal of attention in recent years. One of the most profound effects during femtosecond filamentation is intensity clamping phenomena. It was observed in 1995 by Braun *et al.*[17] that the pulse energy inside a filament is generally constant within long propagation distances. Kasparian *et al.*[18] firstly proposed intensity clamping in 2000. Intensity clamping has a significant impact on the diameter and length of the filament[19]. The gas density effect on filamentation has been investigated[20,21]. The simulation by Geints *et al.*[20] shows that lowering the air pressure in the focusing zone can improve the highest attainable laser pulse intensity by an order of magnitude. The molecular number density of a gas varies with pressure, changing medium properties and affecting the filamentation process. However, Couairon *et al.*[21] numerically investigated filamentation at various air pressures by varying the parameters of the pulse in the propagation model. They found that the clamping intensity is insensitive to pressure. The pulse cumulative effect by high-repetition-rate lasers can also influence the local gas density in the filamentation region. After filamentation, the plasma will recombine rapidly, accompanied by the generation of shock waves and heat. Finally a 'low-density hole' is formed in the filament zone[22,23]. The low-density region will evolve at the rate of air molecule thermal diffusion, that is, up to milliseconds[24]. The low-density hole can be accumulated by pulses. As high-energy, ultrashort, high-repetition-rate laser systems become commercially available,

Correspondence to: Yaoxiang Liu and Tie-Jun Wang, State Key Laboratory of High Field Laser Physics, Shanghai Institute of Optics and Fine Mechanics and CAS Center for Excellence in Ultra-intense Laser Science, Chinese Academy of Sciences, Shanghai 201800, China. Email: yaoxiangliu@siom.ac.cn (Y. Liu); tiejunwang@siom.ac.cn (T.-J. Wang)

© The Author(s), 2023. Published by Cambridge University Press in association with Chinese Laser Press. This is an Open Access article, distributed under the terms of the Creative Commons Attribution licence (http://creativecommons.org/licenses/by/4.0), which permits unrestricted re-use, distribution and reproduction, provided the original article is properly cited.

research on the cumulative effects at repetition rates up to the kHz range can be experimentally achieved. The cumulative effects on filament-related applications of THz generation[25], wake dynamics[26] and the fluorescence[27] have been recently reported. However, the cumulative effect of the laser repetition rate on the intensity inside the filament, which is important to understand and control filament-related applications, is still unclear.

In this work, we look into the problem of the pulse repetition-rate effect on filamentation by both numerical analysis and experimental investigation. It was found that the maximum intensity increases and the filament length extends as the laser repetition rate ranges from 100 to 1000 Hz. A physical picture based on 'low-density hole' dependent laser intensity inside the filament is proposed to explain the clamping intensity variation inside the filament generated by different repetition-rate laser pulses. The clamping intensity of the filament under different repetition rates was experimentally measured in air. The experimental results are in good agreement with the numerical results.

2. Numerical simulations and results

In order to study the influence of low-density holes generated by high repetition-rate lasers on the filamentation process in the steady state, a numerical simulation of ultrashort laser pulse filamentation was performed by solving the nonlinear Schrödinger equation (NLSE) coupled with the electron density evolution equation. The equations are written as follows[28,29]:

$$\frac{\partial E}{\partial z} = i\frac{1}{2k_0}\Delta_\perp E - i\frac{k''}{2}\frac{\partial^2 E}{\partial t^2} + i\frac{\omega_0}{c}n_2 IE - \frac{\beta^K}{2}I^{K-1}E - \frac{\sigma}{2}(1+i\omega_0\tau)\rho E + ik_0\Delta nE, \tag{1}$$

$$\frac{\partial \rho}{\partial t} = \frac{\beta^K}{K\hbar\omega_0}\left(1-\frac{\rho}{\rho_{\text{air}}}\right)I^K, \tag{2}$$

where E is the envelope of the electric field and is assumed to be cylindrically symmetrical around the propagation axis z, $k_0 = 2\pi/\lambda_0$ and $\omega_0 = 2\pi c/\lambda_0$ are the center wave number and center angular frequency for the input laser pulse at the center wavelength $\lambda_0 = 800$ nm, respectively, $I = c\varepsilon_0 n_0|E|^2/2$ is the intensity of the light field and ε_0 is the permittivity in free space. The right-hand terms of Equation (1) account for the diffraction in the transverse plane, group velocity dispersion, Kerr effect, multiphoton absorption, plasma absorption and defocusing with electron density ρ[30] and the refractive index change induced by the preformed density hole.

The heating process caused by filamentation can be regarded as an isochoric (constant volume) process since the pulse transit time (~ps) and the thermalization time (~ps) are much shorter than the timescale of the air flow motion[31]; the peak temperature variation ΔT_{peak} caused by the heat release from the plasma in air is written as follows[32]:

$$\Delta T_{\text{peak}}(z) = \frac{U\rho_{\text{plasma}}(r=0,z)}{c_{\text{v}}\rho_{\text{at}}}, \tag{3}$$

where $U = 14.6$ eV is the ionization potential energy for the air molecules, $\rho_{\text{plasma}}(z)$ is the longitudinal distribution of plasma density in the single-pulse case and c_{v} is the gas isochoric heat capacity per molecule. The ambient air under 1 atm can be approximately regarded as an ideal diatomic molecular gas and $c_{\text{v}} = 5k_{\text{B}}/2$. Here, $k_{\text{B}} = 1.38\times10^{-23}$ J/K is the Boltzmann constant and ρ_{at} is the neutral molecule density in the air under 1 atm.

The air density of the density hole induced by the energy deposition in the air is written as follows[33]:

$$\rho_{\text{air}}(z) = \rho_{\text{at}} - \Delta\rho_{\text{air}}^{\text{peak}}(z)\exp\left(-\frac{r^2}{R(z)^2}\right), \tag{4}$$

$$\Delta\rho_{\text{air}}^{\text{peak}}(z) = \rho_{\text{at}}\frac{\Delta T_{\text{peak}}(z)R_0^2(z)}{\left(\Delta T_{\text{peak}}(z)+T_{\text{a}}\right)R^2(z)}, \tag{5}$$

where $T_{\text{a}} = 300$ K is the ambient air temperature and $R(z) = \left(R_0^2(z)+4\alpha\Delta t\right)^{1/2}$ is the radius of the density hole. The initial radius of the density hole $R_0(z)$ is the radial distribution of plasma density in full width at half-maximum (FWHM) at the z position. Then the 'low-density hole' will evolve with the thermal diffusivity $\alpha = 0.19$ cm^2/s[33,34]. Here, Δt is the pulse temporal spacing of the subsequent pulse.

The values given above correspond to the neutral molecule density of the air under 1 atm. Some of the parameters in Equation (1) vary with the air density. The variations with the molecule density of air are as follows[21]:

$$n_2 = n_{2,0}\times\rho_{\text{index}},\ \tau = \tau_0/\rho_{\text{index}},\ \sigma = \sigma_0\times\frac{\rho_{\text{index}}\left(1+\omega_0^2\tau_0^2\right)}{\rho_{\text{index}}^2+\omega_0^2\tau_0^2},$$
$$\beta^K = \beta_0^K\times\rho_{\text{index}},\ k'' = k_0''\times\rho_{\text{index}}, \tag{6}$$

where $\rho_{\text{index}} = \rho_{\text{air}}/\rho_{\text{at}}$ denotes the relative air density. In the case of the ambient air under 1 atm, $n_{2,0} = 3.2\times10^{-23}$ m^2/W is the nonlinear coefficient of the Kerr effect, $\tau_0 = 350$ fs is the momentum transfer collision time, $\sigma_0 = 2\times10^{-24}$ m^2 is the cross-section for inverse bremsstrahlung, $\beta_0^K = 1.27\times10^{-160}$ m^{17}/W^9 is the coefficient related to the multiphoton ionization and $k_0'' = 2\times10^{-29}$ s^2/m is the coefficient of group velocity dispersion.

The density hole induces the refractive index change, which is written as follows[34]:

$$\Delta n(z) = -\Delta n_{\text{m}}(z)\exp\left(-\frac{r^2}{R^2(z)}\right), \tag{7}$$

$$\Delta n_{\mathrm{m}}(z) = (n_0 - 1)\,\frac{\Delta T_{\mathrm{peak}}(z)}{T_{\mathrm{a}}}\frac{R_0^2(z)}{R^2(z)}, \tag{8}$$

where $n_0 = 1.000275$ is the refractive index of the ambient air and Δn_{m} is the maximal refractive index change[34].

To reduce computer processing time, the simulations begin at $d = 5.2$ cm before the linear (geometrical) focus[35]. The initial laser beam is assumed to be Gaussian, which can be expressed as follows:

$$E = E_0 \exp\left(-r^2/w_0^2\right) \exp\left(-t^2/\tau_{\mathrm{p}}^2\right) \exp\left(-ik_0 r^2/2f\right), \tag{9}$$

where $w_0 = w_{\mathrm{f}}/\left(1 + d^2/z_{\mathrm{f}}^2\right)^{1/2}$ and $\tau_{\mathrm{p}} = 35$ fs are the transverse waist and the duration of the Gaussian beam, respectively. Here, $w_{\mathrm{f}} = 7$ mm is the beam waist (1/e) before the focus lens, $z_{\mathrm{f}} = \pi w_{\mathrm{f}}^2 n_0/\lambda_0$ is the Rayleigh length of the beam and $f = d + z_{\mathrm{f}}^2/d$ is the curvature of the laser wave at the distance d before the linear focus.

The NLSE (Equation (1)) was solved by the split-step Crank–Nicolson method[35]. Figure 1 shows the simulation results of the maximal intensity of the femtosecond laser pulse as a function of the propagation distance under laser repetition rates of 100 and 1000 Hz. When the pulse energy is low, for example, 0.1 mJ, the laser filament is not formed yet. The repetition-rate effect appears mainly around the geometrical focus (Figure 1(a)). When the pulse energy is high enough for filamentation, the effect appears not only around the peak but also on the tailing edge of the filament (Figures 1(b)–1(d)). Compared with the result of the 100 Hz laser pulse, the maximal intensity is higher for the 1000 Hz laser pulse at both the peak and tailing edge of the filament, while there is less influence at the leading edge of the filament. The length of the filament generated by the 1000 Hz laser pulse is longer than that by the 100 Hz laser pulse (Figure 1).

3. Experimental setup and results

In order to confirm the simulation results, the experiments of femtosecond laser filamentation in air under 100 and 1000 Hz pulse repetition rates were performed. The simple

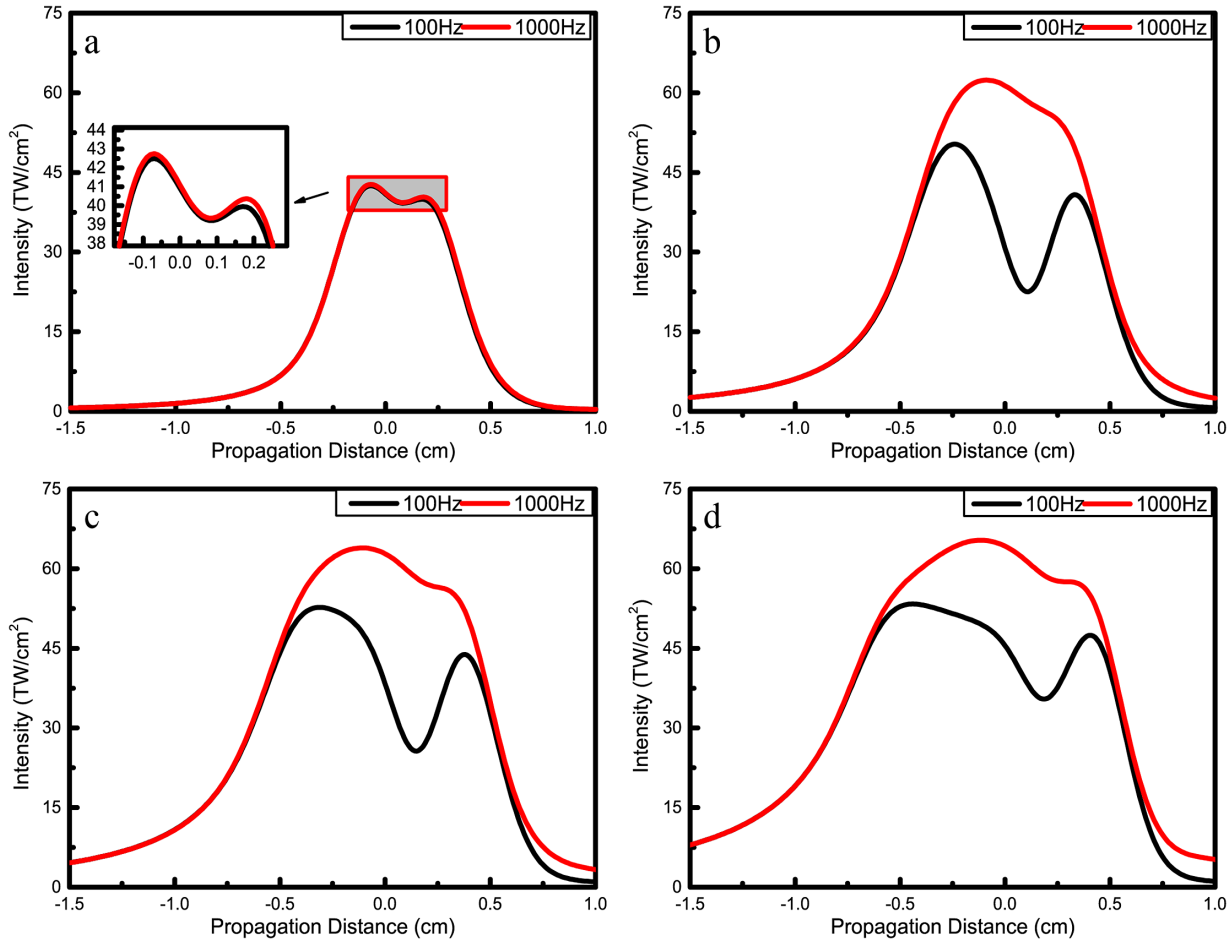

Figure 1. Maximal on-axis intensities of femtosecond laser pulses as a function of propagation distance for 100 and 1000 Hz repetition rates with different pulse energies of (a) 0.1 mJ, (b) 0.2 mJ, (c) 0.7 mJ and (d) 1.2 mJ. The geometric focus position is defined as 0 of the propagation distance and the negative values are before the focus. The inset of (a) shows the enlargement of the shadow region of (a).

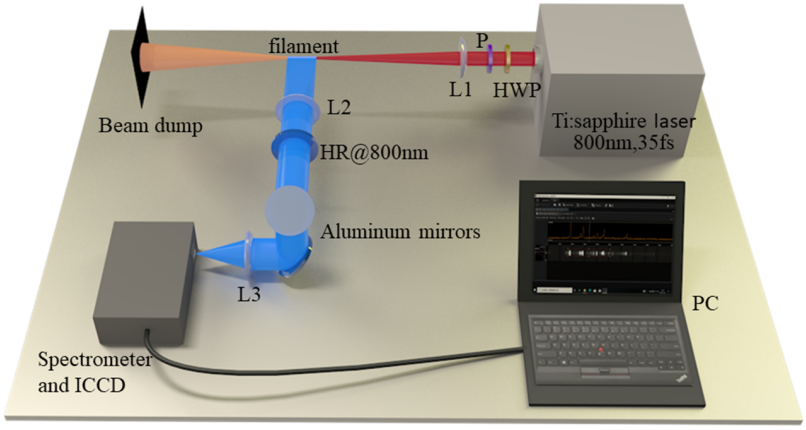

Figure 2. Experimental setup.

fluorescence-based method reported by Xu *et al.*[36] was adapted to estimate the laser peak intensity inside the filament in air. The experimental setup is shown in Figure 2. A femtosecond laser pulse (800 nm/4 Hz to 1 kHz/35 fs) generated by a Ti:sapphire (chirped pulse amplification (CPA)) system (Spitfire Ace, Spectral-Physics) was focused by a fused silica convex lens L1 (f = 30 cm). The radius of the laser beam waist is about 7 mm (1/e). The input energy of the laser pulse is continuously adjusted by a combination of a polarizer, P, and a half-wave plate, HWP. The fluorescence emitted by the filament was imaged from the side by an imaging system of a pair of lenses L2 and L3 (30 and 10 cm focal lengths) and a pair of orthogonal ultraviolet-enhanced aluminum mirrors into the slit of a spectrometer. An intensified charge-coupled device (ICCD) mounted on the spectrometer trigged by the laser system was used to record the fluorescence spectrum generated from the filament. An energy meter (OPHIR PE50-DIF-C) inserted after L1 was employed to precisely monitor the laser energy under different repetition rates.

The typical fluorescence images of the laser filament on the ICCD are shown in Figure 3 for the laser pulse energy of 1.2 mJ and repetition rate of 1000 Hz. The images of the fluorescence spectra around 337 and 391 nm from the filament were acquired and were used for laser intensity estimation.

The longitudinal distributions of the two fluorescence lines in Figure 3 are shown in Figure 4 for laser repetition rates of 100 and 1000 Hz. The laser pulse energy was fixed at 1.2 mJ. In Figure 4, the distance range that the 391 nm fluorescence covers is smaller than that of the 337 nm signal. The distance ranges of the two fluorescence signals are enlarged with the increasing repetition rate of the laser pulses. The relevant effects of the 'density hole' induced by the previous pulse, such as the thermal lens, will weaken the external focus

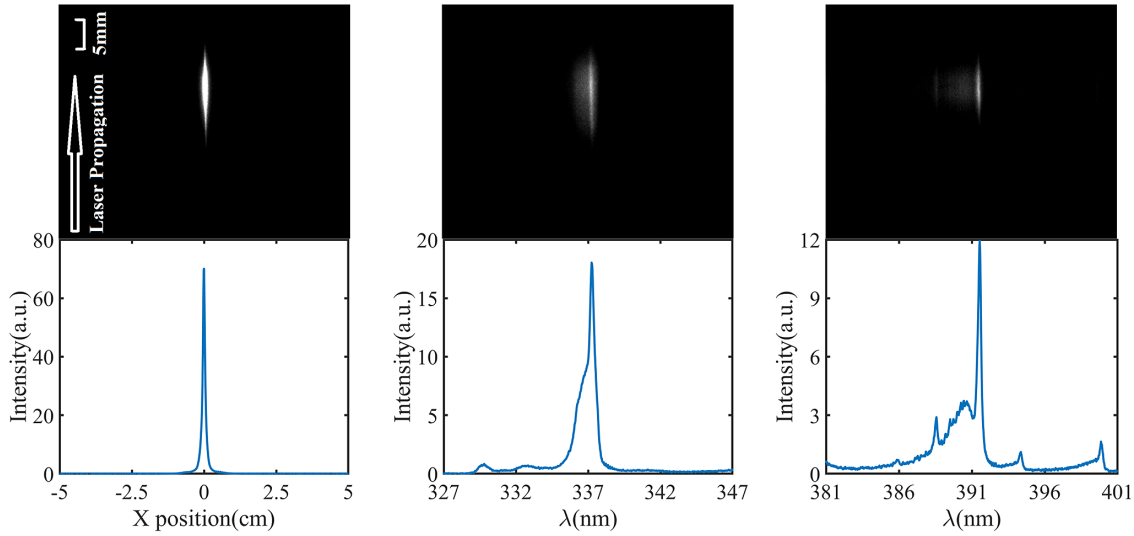

Figure 3. The typical spectrum images and intensity plots captured by the ICCD mounted on the spectrometer: (a) is in non-divided imaging mode, while (b) and (c) are centered at the wavelengths of 337 and 391 nm, respectively. The laser pulse energy and repetition rate are 1.2 mJ and 1000 Hz, respectively.

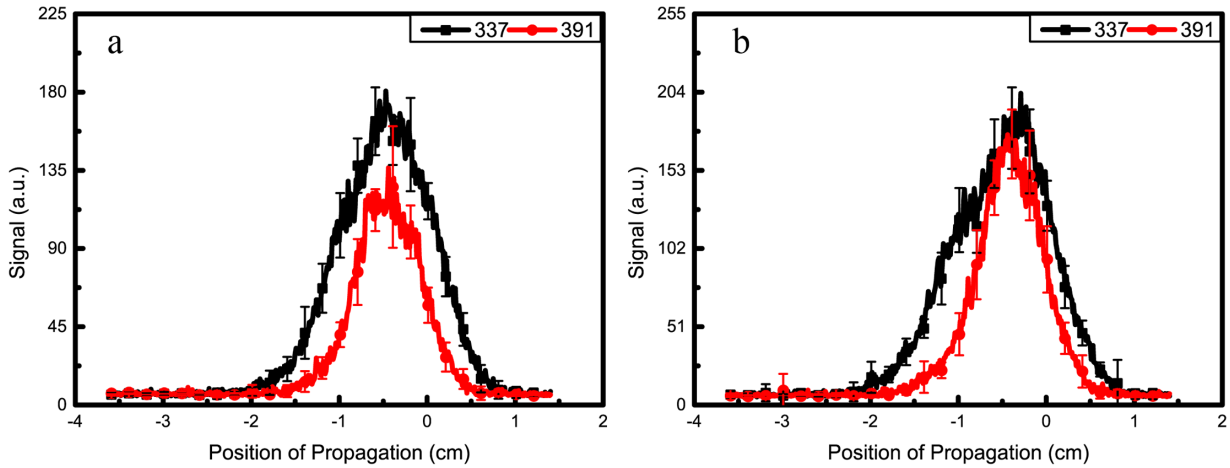

Figure 4. Longitudinal distribution of the nitrogen 337 and 391 nm fluorescence signal along the filaments under filament repetition rates of (a) 100 Hz and (b) 1000 Hz. The geometric focus position is defined as 0 of the propagation position and the negative values are before the focus. The laser pulse energy is 1.2 mJ for filamentation.

and reduce the consumption of laser energy through air ionization. As a consequence, longer filaments as predicted in the simulation (Figure 1) were experimentally observed (Figure 4). A higher laser repetition rate, which means a shorter pulse interval, leads to a stronger effect on filament length.

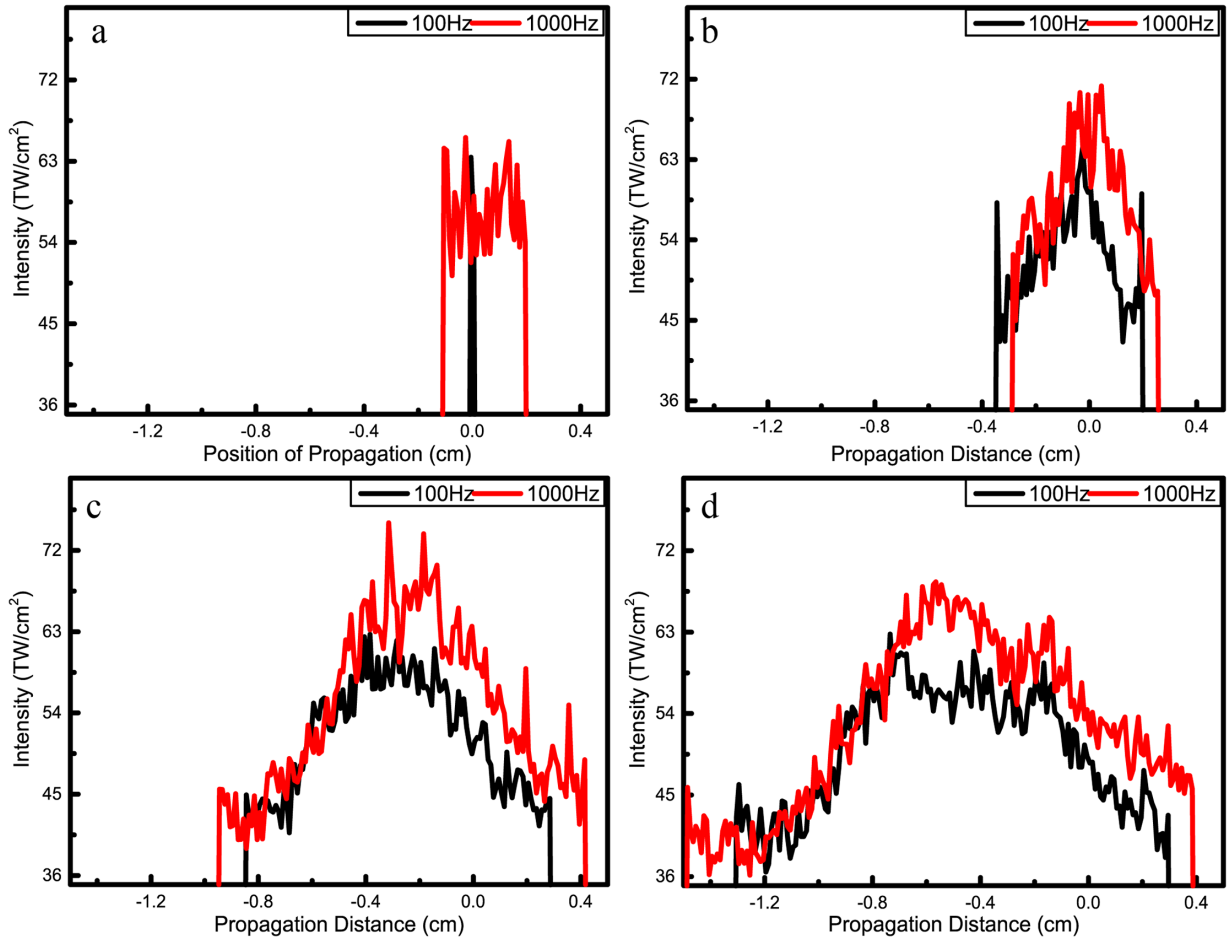

Figure 5. The laser peak intensities with different incident laser pulse energies of (a) 0.1 mJ, (b) 0.2 mJ, (c) 0.7 mJ and (d) 1.2 mJ under different laser repetition rates (black line, 100 Hz; red line, 1 kHz), as determined by Equation (10).

To characterize the laser intensity inside the filament, we use the empirical formula reported in Ref. [36], which is based on the 391 and 337 nm nitrogen fluorescence as follows:

$$I = 79 \times \left(\frac{2.6}{R} - 1\right)^{-0.34} \text{TW/cm}^2, \tag{10}$$

where $R \equiv \frac{S_{391}}{S_{337}} \propto \frac{aI^{n_1}}{aI^{n_1}+bI^{n_2}}$ is the intensity ratio between the two fluorescence lines, I is the pulse peak intensity, n_1, n_2 are the effective orders of nonlinearity of ionizing the molecule into the excited or ground state ions and a, b are the proportionality constants. The laser peak intensity could be calculated using the value of R through Equation (10).

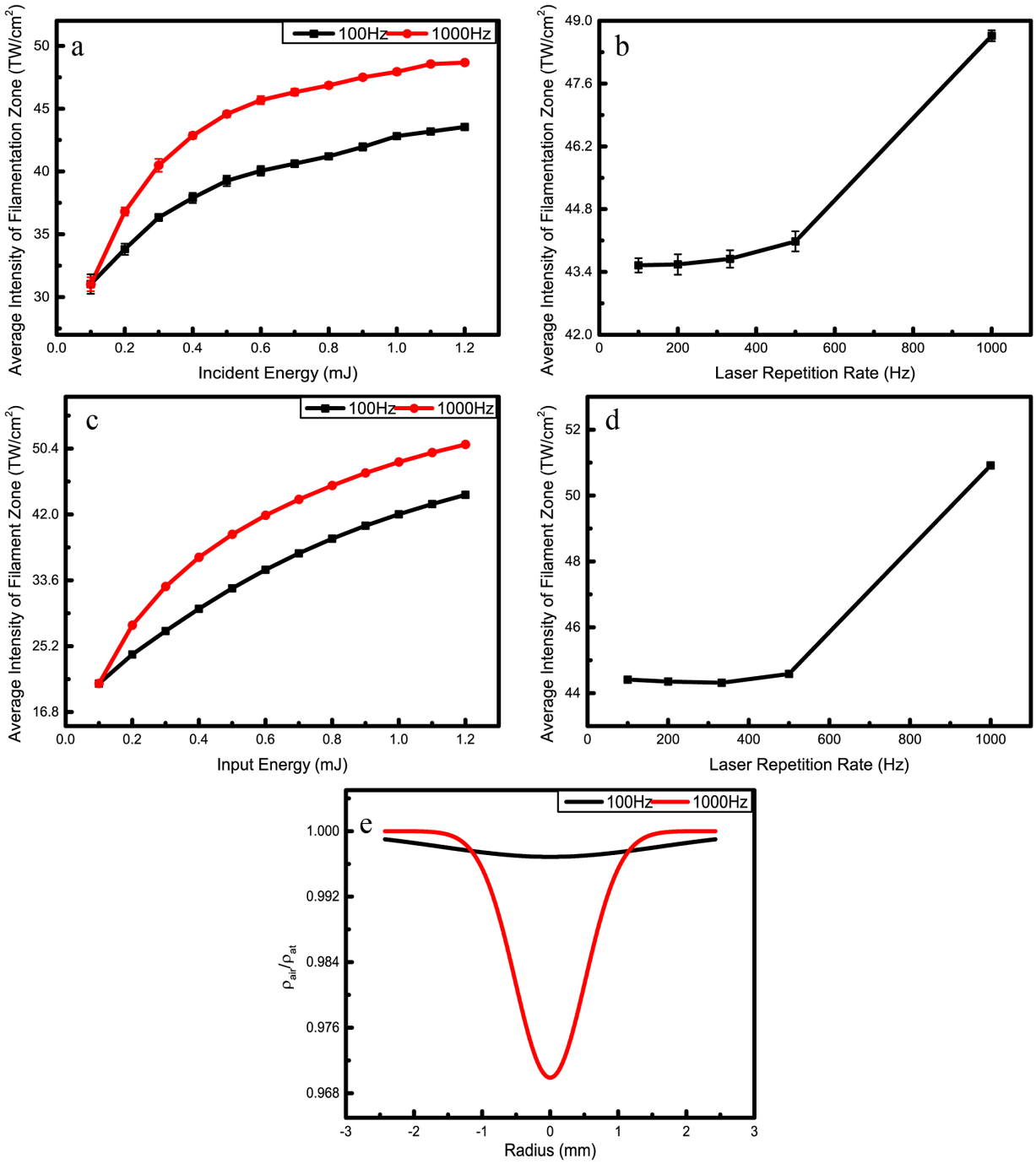

Figure 6. Experimentally measured average intensity of the filament as a function of (a) incident energy and (b) laser repetition rate (the incident energy is 1.2 mJ). The filament range is defined by specifying the filamentation initiation and termination when the total fluorescence intensity approaches 1/e of the maximum intensity. (c) Numerically obtained average intensity of the filamentation zone as a function of incident energy for laser repetition rates of 100 and 1000 Hz. (d) Numerically obtained average intensity of the filamentation zone as a function of laser repetition rates for incident energy of 1.2 mJ. (e) The radial distributions of the gas density hole generated by 100 and 1000 Hz repetition-rate lasers.

Figure 5 depicts the experimentally measured laser peak intensity as a function of propagation under different laser pulse energies of 0.1, 0.2, 0.7 and 1.2 mJ, respectively. At the low energy of 0.1 mJ, the fluorescence-based intensity estimation method does not reproduce the simulation prediction due to the weak fluorescence excited at the small energy (Figure 5(a)). Once laser pulse energy is high enough for filamentation, the predicted intensity behaviors under 100 and 1000 Hz pulse repetition rates are well reproduced (Figures 5(b)–5(d)). No clear differences in intensity at the leading edges of the filaments were observed, which agrees with the simulation results in Figures 1(b)–1(d). During the filamentation process, the laser peak intensity is approximately 70 TW/cm^2. The laser peak intensity is stronger and the filamentation zone is enlarged when using a higher laser repetition rate of 1000 Hz. The experimental results are well consistent with the numerical simulations based on the NLSE.

Figure 6(a) depicts the experimentally acquired average intensity of the filamentation zone for all incident energies. The filament zone is defined by specifying the filamentation initiation and termination when the total fluorescence intensity approaches 1/e of the maximum intensity. The intensity tends to be saturated because of the clamping effect when the incident energy increases. Furthermore, the obtained intensities of the 1 kHz filament are higher than those of 100 Hz. Figure 6(b) summarizes the average intensity of the filamentation zone, demonstrating the intensity inside the filament as a function of the laser repetition rate. For comparison, the numerically obtained average intensity of the filamentation zone as a function of laser input energy is shown in Figure 6(c). Both experimental and theoretical results show that the average intensity of the 1000 Hz filament is clearly higher than that of the 100 Hz filament. The difference enlarges as the laser pulse energy increases. The experimental results are in good agreement with those predicted by the simulation in Figures 6(c) and 6(d), which confirms that the repetition-rate dependent low-density hole plays a significant role during filamentation in air.

The effect of the pulse repetition rate on filamentation can be understood as the following. After the recombination of the plasmas inside the filament zone, part of the laser pulse energy is deposited into air molecules, resulting in thermal diffusion along the radial direction. As a consequence, a low-density hole in air is established. The density hole decays in a millisecond timescale[24] and the next pulse will 'see' it if the pulse interval time is shorter than the density hole lifetime. The 'density hole' impacts the laser filament in two ways. One is to change the spatial distribution of the air refractive index. The refractive index distribution structure acts like a defocus lens, namely a thermal lens, weakening the focus of the succeeding laser pulse. The other is to influence other parameters of the air medium, such as the nonlinear Kerr effect coefficient, the momentum transfer collision time, the cross-section for inverse bremsstrahlung, the coefficient linked to multiphoton ionization and the coefficient of group velocity dispersion. These parameters play an important role in laser pulse nonlinear propagation (Equation (1)). The time for the 'density hole' to decay is 1 and 10 ms for laser repetition rates of 1 kHz and 100 Hz, respectively. The radius of the steady 'density hole' is smaller for 1 kHz (Figure 6(e)), which induces larger maximum refractive shifts. The density hole caused by the previous pulse at 1000 Hz is sharper than that at 100 Hz, due to the shorter pulse interval time of 1 ms, as shown in Figure 6(e). The next subsequent pulse propagating in the region experiences a smaller nonlinear refractive index coefficient and lower ionization rate for a higher repetition-rate laser. As a consequence, less energy is consumed by tunneling/multiphoton ionization and thus more energy is confined in the filament region. Therefore, the clamped intensity of the laser filaments increases when using a higher repetition-rate laser (Figures 6(a)–6(d)). At the leading edge of filament, the plasma density is not that high compared with that at the peak and the tailing of the filament. Therefore, less energy is deposited in the region through plasma recombination, leading to very weak thermal lensing effect. This could contribute to less laser repetition influence at the leading edge of the filaments in Figure 1. The peak power at the position of the previous filament tail is still high enough for self-focusing as well as for filamentation, which leads to the extension of the filament length at the tail end, both experimentally and theoretically.

It is noted that more recently Isaacs *et al*.[37] developed a model describing pulse train isobaric heating air, and simulated the propagation of a high-power pulse train at a 1 kHz repetition rate. Similar results of the filament length are predicted by the model when the pulse cumulative effect is considered. However, no obvious change of the peak intensity inside the laser filament was predicted, since only the refractive index change caused by the 'low-density hole' was considered in the model.

4. Conclusion

In summary, the theoretical and experimental investigations on pulse repetition-rate dependent laser filamentation in air were performed. The numerical prediction results by solving the NLSE reveal that the maximum intensity inside the filament is higher and the length of the filament is longer for a 1000 Hz laser pulse compared with the result by a 100 Hz pulse. The pulse repetition-rate effect has a negligible influence at the leading edge of the laser filament. Clear intensity enhancement from the high-repetition pulse is observed at the peak and tailing edges of the laser filament. The formation of a 'low-density hole' after filamentation by the last pulse leads to a defocusing effect and lower ionization rate. For laser pulses at a high repetition rate, the density hole caused by the previous pulse is sharper

than that at a low repetition rate due to the shorter pulse interval time. Consequently, the clamped laser intensity of the laser filaments is higher with a higher repetition rate. Direct experimental measurements of the laser peak intensity of different incident laser pulse energies under different laser repetition rates were performed via the side fluorescence of the filament. Using the image of the spectrum of the side fluorescence from the filament, the longitudinal distribution of the laser peak intensity of the filament was resolved. The experimental results are in good agreement with the numerical predictions. We believe that the results presented in this work are useful not only for further understanding the laser repetition effect on the laser filamentation in air, but also for related applications.

Acknowledgement

The work was in part supported by the NSAF (No. U2130123), the International Partnership Program of the Chinese Academy of Sciences (Nos. 181231KYSB20200033 and 181231KYSB20200040) and the Shanghai Science and Technology Program (No. 21511105000).

References

1. S. L. Chin, S. A. Hosseini, W. Liu, Q. Luo, F. Théberge, N. Aközbek, A. Becker, V. P. Kandidov, O. G. Kosareva, and H. Schroeder, Canad. J. Phys. **83**, 863 (2005).
2. S. L. Chin, T.-J. Wang, C. Marceau, J. Wu, J. S. Liu, O. Kosareva, N. Panov, Y. P. Chen, J.-F. Daigle, S. Yuan, A. Azarm, W. W. Liu, T. Seideman, H. P. Zeng, M. Richardson, R. Li, and Z. Z. Xu, Laser Phys. **22**, 1 (2012).
3. A. Couairon and A. Mysyrowicz, Phys. Rep. **441**, 47 (2007).
4. L. Bergé, S. Skupin, G. Méjean, J. Kasparian, J. Yu, S. Frey, E. Salmon, and J. P. Wolf, Phys. Rev. E **71**, 016602 (2005).
5. A. K. Dharmadhikari, S. Edward, J. A. Dharmadhikari, and D. Mathur, J. Phys. B **48**, 094012 (2015).
6. N. Chen, T.-J. Wang, Z. Zhu, H. Guo, Y. Liu, F. Yin, H. Sun, Y. Leng, and R. Li, Opt. Lett. **45**, 4444 (2020).
7. N. Aközbek, A. Iwasaki, A. Becker, M. Scalora, S. L. Chin, and C. M. Bowden, Phys. Rev. Lett. **89**, 143901 (2002).
8. D. Wang, W. Li, L. Ding, and H. Zeng, Opt. Lett. **39**, 4140 (2014).
9. L. Yuan, Y. Liu, J. Yao, and Y. Cheng, Adv. Quantum Tech. **2**, 1900080 (2019).
10. P. Polynkin and Y. Cheng, eds., *Air Lasing*, Springer Series in Optical Sciences (Springer International Publishing, Cham, 2018), Vol. **208**.
11. T.-J. Wang, J. Ju, Y. Liu, R. Li, Z. Xu, and S. L. Chin, Appl. Phys. Lett. **110**, 221102 (2017).
12. C. D'Amico, A. Houard, M. Franco, B. Prade, A. Mysyrowicz, A. Couairon, and V. T. Tikhonchuk, Phys. Rev. Lett. **98**, 235002 (2007).
13. H. L. Xu, J. F. Daigle, Q. Luo, and S. L. Chin, Appl. Phys. B **82**, 655 (2006).
14. Y. Wei, Y. Liu, T.-J. Wang, N. Chen, J. Ju, Y. Liu, H. Sun, C. Wang, J. Liu, H. Lu, S. L. Chin, and R. Li, High Power Laser Sci. Eng. **4**, e8 (2016).
15. C. Hnatovsky, V. Shvedov, W. Krolikowski, and A. Rode, Phys. Rev. Lett. **106**, 123901 (2011).
16. J. Ju, T. Leisner, H. Sun, A. Sridharan, T.-J. Wang, J. Wang, C. Wang, J. Liu, R. Li, Z. Xu, and S. L. Chin, Appl. Phys. B **117**, 1001 (2014).
17. A. Braun, G. Korn, X. Liu, D. Du, J. Squier, and G. Mourou, Opt. Lett. **20**, 3 (1995).
18. J. Kasparian, R. Sauerbrey, and S. L. Chin, Appl. Phys. B **71**, 877 (2000).
19. S. Hosseini, O. Kosareva, N. Panov, V. P. Kandidov, A. Azarm, J.-F. Daigle, A. B. Savel'ev, T.-J. Wang, and S. L. Chin, Laser Phys. Lett. **9**, 868 (2012).
20. Y. E. Geints, A. A. Zemlyanov, A. A. Ionin, S. I. Kudryashov, L. V. Seleznev, D. V. Sinitsyn, and E. S. Sunchugasheva, Quantum Electron. **42**, 319 (2012).
21. A. Couairon, M. Franco, G. Méchain, T. Olivier, B. Prade, and A. Mysyrowicz, Opt. Commun. **259**, 265 (2006).
22. J. K. Wahlstrand, N. Jhajj, E. W. Rosenthal, S. Zahedpour, and H. M. Milchberg, Opt. Lett. **39**, 1290 (2014).
23. N. Jhajj, Y.-H. Cheng, J. K. Wahlstrand, and H. M. Milchberg, Opt. Express **21**, 28980 (2013).
24. G. Point, C. Milián, A. Couairon, A. Mysyrowicz, and A. Houard, J. Phys. B **48**, 094009 (2015).
25. A. D. Koulouklidis, C. Lanara, C. Daskalaki, V. Y. Fedorov, and S. Tzortzakis, Opt. Lett. **45**, 6835 (2020).
26. A. Higginson, Y. Wang, H. Chi, A. Goffin, I. Larkin, H. M. Milchberg, and J. J. Rocca, Opt. Lett. **46**, 5449 (2021).
27. J. Xue, N. Zhang, L. Guo, Z. Zhang, P. Qi, L. Sun, C. Gong, L. Lin, and W. Liu, Opt. Lett. **47**, 5676 (2022).
28. J. Chang, D. Li, L. Xu, L. Zhang, T. Xi, and Z. Hao, Opt. Express **30**, 16987 (2022).
29. A. Couairon, E. Brambilla, T. Corti, D. Majus, O. de J. Ramírez-Góngora, and M. Kolesik, Eur. Phys. J. Spec. Top. **199**, 5 (2011).
30. E. Yablonovitch and N. Bloembergen, Phys. Rev. Lett. **29**, 907 (1972).
31. G. Point, E. Thouin, A. Mysyrowicz, and A. Houard, Opt. Express **24**, 6271 (2016).
32. Q. Zeng, L. Liu, J. Ju, S. Hu, and K. Zhang, Phys. Scr. **95**, 085605 (2020).
33. Y.-H. Cheng, J. K. Wahlstrand, N. Jhajj, and H. M. Milchberg, Opt. Express **21**, 4740 (2013).
34. J. K. Wahlstrand, N. Jhajj, and H. M. Milchberg, Opt. Lett. **44**, 199 (2019).
35. H. Guo, T.-J. Wang, X. Zhang, C. Liu, N. Chen, Y. Liu, H. Sun, B. Shen, Y. Jin, Y. Leng, and R. Li, Opt. Express **28**, 15529 (2020).
36. S. Xu, X. Sun, B. Zeng, W. Chu, J. Zhao, W. Liu, Y. Cheng, Z. Xu, and S. L. Chin, Opt. Express **20**, 299 (2012).
37. J. Isaacs, B. Hafizi, L. A. Johnson, E. W. Rosenthal, L. Mrini, and J. Peñano, Opt. Express **30**, 22306 (2022).